PLOS BIOLOGY

RESEARCH ARTICLE

A non-natural nucleotide uses a specific pocket to selectively inhibit telomerase activity

Wilnelly Hernandez-Sanchez[1], Wei Huang[1], Brian Plucinsky[2], Nelson Garcia-Vazquez[1], Nathaniel J. Robinson[3], William P. Schiemann[4], Anthony J. Berdis[5], Emmanuel Skordalakes[2], Derek J. Taylor[1,6]*

1 Department of Pharmacology, Case Western Reserve University, Cleveland, Ohio, United States of America, **2** The Wistar Institute Gene Expression and Regulation Program, Philadelphia, Pennsylvania, United States of America, **3** Department of Pathology, Case Western Reserve University, Cleveland, Ohio, United States of America, **4** Case Comprehensive Cancer Center, Case Western Reserve University, Cleveland, Ohio, United States of America, **5** Department of Chemistry, Cleveland State University, Cleveland, Ohio, United States of America, **6** Department of Biochemistry, Case Western Reserve University, Cleveland, Ohio, United States of America

* derek.taylor@case.edu

Citation: Hernandez-Sanchez W, Huang W, Plucinsky B, Garcia-Vazquez N, Robinson NJ, Schiemann WP, et al. (2019) A non-natural nucleotide uses a specific pocket to selectively inhibit telomerase activity. PLoS Biol 17(4): e3000204. https://doi.org/10.1371/journal.pbio.3000204

Academic Editor: Agata Smogorzewska, The Rockefeller University, UNITED STATES

Received: August 24, 2018

Accepted: March 14, 2019

Published: April 5, 2019

Data Availability Statement: All relevant data are within the paper and its Supporting Information files. The structural model has been deposited in the RCSB with accession number 6E53.

Funding: This work was funded by National Institutes of Health DP2 CA186571 (DJT), National Institutes of Health R01 CA201312 (ES), and American Cancer Society RSG-13-211-01-DMC (DJT). The funders had no role in study design,

Abstract

Telomerase, a unique reverse transcriptase that specifically extends the ends of linear chromosomes, is up-regulated in the vast majority of cancer cells. Here, we show that an indole nucleotide analog, 5-methylcarboxyl-indolyl-2′-deoxyriboside 5′-triphosphate (5-MeCITP), functions as an inhibitor of telomerase activity. The crystal structure of 5-MeCITP bound to the *Tribolium castaneum* telomerase reverse transcriptase reveals an atypical interaction, in which the nucleobase is flipped in the active site. In this orientation, the methoxy group of 5-MeCITP extends out of the canonical active site to interact with a telomerase-specific hydrophobic pocket formed by motifs 1 and 2 in the fingers domain and T-motif in the RNA-binding domain of the telomerase reverse transcriptase. In vitro data show that 5-MeCITP inhibits telomerase with a similar potency as the clinically administered nucleoside analog reverse transcriptase inhibitor azidothymidine (AZT). In addition, cell-based studies show that treatment with the cell-permeable nucleoside counterpart of 5-MeCITP leads to telomere shortening in telomerase-positive cancer cells, while resulting in significantly lower cytotoxic effects in telomerase-negative cell lines when compared with AZT treatment.

Introduction

Linear chromosomes end in telomeres, which are repetitive G-rich sequences (TTAGGG in mammals) that guard against illicit DNA repair and end-to-end fusions [1,2]. Because replicative DNA polymerases operate directionally, they are unable to fully synthesize the end of the lagging strand of DNA [3]. Telomeres function to absorb the shortening that occurs at each cell division and, thus, protect against the loss of genetic information. The progressive shortening of telomeres restricts the number of times a cell will divide until a state of replicative

data collection and analysis, decision to publish, or preparation of the manuscript.

Competing interests: The authors have declared that no competing interests exist.

Abbreviations: ALT, alternative lengthening of telomeres; AZT, azidothymidine; AZT-TP, AZT triphosphate; dATP, deoxyadenosine triphosphate; dG, deoxyguanosine; dGTP, deoxyguanosine triphosphate; dNTP, deoxynucleoside triphosphate; DMEM, Dulbecco's Modified Eagle Medium; dTTP, deoxythymidine triphosphate; FBS, fetal bovine serum; $K'_{1/2}$, apparent rate constant; $K_{1/2}$, relative rate constant; MR, molecular replacement; NRTI, nucleoside reverse transcriptase inhibitor; RT, reverse transcriptase; ssDNA, single stranded DNA; TBE, template boundary element; TERT, telomerase reverse transcriptase; TR, telomerase RNA template; TRBD, telomerase RNA-binding domain; TRF, telomere restriction fragment; 4-NITP, 4-nitroindolyl-2′-deoxyriboside 5′-triphosphate; 5-CITP, 5-carboxylindolyl-2′-deoxyriboside 5′-triphosphate; 5-EyITP, 5-ethyleneindolyl-2′-deoxyriboside 5′-triphosphate; 5-FITP, 5-fluoroindolyl-2′-deoxyriboside 5′-triphosphate; 5-MeCIdR, cell-permeable nucleoside form of 5-MeCITP; 5-MeCITP, 5-methylcarboxyl-indolyl-2′-deoxyriboside 5′-triphosphate; 5-MeITP, 5-methylindolyl-2′-deoxyriboside 5′-triphosphate; 6-NITP, 6-nitroindolyl-2′-deoxyriboside 5′-triphosphate.

senescence is induced, known as the Hayflick limit [4]. In highly proliferative tissues (e.g., during embryogenesis, germline and stem cells), telomerase, the enzyme that synthesizes telomere ends, is reactivated to extend telomere DNA to counterbalance telomere attrition [5]. Telomerase activity is undetectable in healthy somatic cells but is reactivated in 90% of all cancer cells, thereby driving tumorigenesis [6]. Because of this distinction, the inhibition of telomerase activity is a promising therapeutic strategy for many cancers.

Telomerase is a multicomponent, ribonucleoprotein enzyme that includes a catalytic telomerase reverse transcriptase (TERT) protein and a noncoding RNA molecule that serves as the template for synthesis of telomere DNA [7–9]. The genetic removal or pharmacological inhibition of telomerase results in sequential telomere shortening that eventually triggers senescence or apoptosis in cancer cells [10]. Among telomerase antagonists that have been developed, Imetelstat (GRN163L) is one of the most studied for its clinical application. Imetelstat is a lipid conjugated–modified oligonucleotide that is designed to impair telomerase activity by hybridizing with its template RNA [11]. A primary limitation of Imetelstat administration has been attributed to nonspecific interactions that are coordinated through the lipid moiety, which increases off-target effects [12]. Thus, the development of alternative small-molecule compounds that do not involve lipid conjugation will provide benefits for the administration of telomerase-dependent therapeutic approaches.

The use of soluble nucleoside analogs has provided a promising strategy for targeting reverse transcriptase (RT) enzymes that include telomerase. Nucleoside analogs represent a large class of compounds that have a successful history as antivirals and in cancer therapy [13,14]. Administered analogs enter cancer cells by nucleoside transporters, where they are phosphorylated by cellular nucleoside kinases to interfere with RNA and DNA synthesis or with nucleotide biogenesis [14,15]. As a primary example, azidothymidine (AZT) is a thymidine analog with clinical success as an RT inhibitor, specifically in the treatment of human immunodeficiency virus (HIV-1) infections [16,17]. Although TERT contains additional domains, its catalytic core is structurally homologous to the RT domain of HIV-1 [18]. Therefore, it is not surprising that nucleoside reverse transcriptase inhibitors (NRTIs) exhibit inhibitory properties against telomerase as well [19–21]. Indeed, AZT treatment has reached Phase II clinical trials as a telomerase inhibitor for the treatment of colorectal cancer [22], pancreatic adenocarcinoma [23], and other malignant tumors [24,25]. Although promising, AZT treatment exhibits significant cytotoxic effects, as it indiscriminately inhibits other DNA polymerases as well [26,27].

Here, we have investigated a set of chemically diverse nucleotide analogs as potential inhibitors of telomerase activity. In doing so, we have identified 5-methylcarboxyl-indolyl-2′-deoxyriboside 5′-triphosphate (5-MeCITP) as an inhibitor of telomerase activity. Structural studies reveal that the analog binds to the TERT active site with the nucleobase inverted so that the methylcarboxyl modification interacts with a telomerase-specific, hydrophobic pocket adjacent to the TERT active site that is formed by motifs 1 and 2 within the fingers domain and the telomerase-specific motif (T-motif) in the telomerase RNA-binding domain (TRBD). The unconventional positioning of 5-MeCITP, along with an inability to form proper Watson-Crick base pairings, results in the displacement of the complementary bases of the RNA template away from the TERT active site. Administration of the cell-permeable form of 5-MeCITP (5-MeCIdR) results in telomerase-dependent telomere shortening in cancer cells. Cumulatively, we identify a nucleotide analog that implements a unique mechanism to selectively inhibit telomerase-mediated extension of telomere DNA.

Results

Screening of indolyl-2′-deoxynucleotide analogs for telomeric incorporation

Telomerase functions as a unique RT that uses a specialized, noncoding RNA as a template for telomere DNA synthesis [9,18,28,29]. This distinctive trait, along with additional differences in sequence, structure, and overall function compared with conventional replicative and repair polymerases [30,31], could provide key features of telomerase that can be exploited therapeutically. Pursuing this potential, we selected a set of indolyl-2′-deoxynucleotide analogs that exhibit different chemical properties and screened them for their ability to inhibit telomerase activity (**Fig 1A** and **S1 Table**). These analogs were designed to mimic the core structure of deoxyadenosine triphosphate (dATP), but with the introduction of various functional groups at the 5- or 6-position of the indole ring to systematically modulate biophysical features such as hydrophobicity, size variation, shape, and π-electron density that might contribute to selective interactions with telomerase. Modification of the nucleobase at these positions will additionally disturb proper Watson-Crick base pairing with the RNA template. Finally, the individual analogs investigated are already known to exhibit differential effects on diverse DNA polymerases that include HIV-1 RT, bacteriophage T4 DNA polymerase, and *Escherichia coli* Klenow fragment [32–36].

Alterations that these artificial nucleotide analogs had on telomerase activity were characterized using a modified direct in vitro telomerase activity assay [37]. Our first set of experiments were designed to determine whether any of the analogs serve as effective substrates for telomerase-mediated extension. As such, the indolyl analogs were used in place of the structurally similar native dATP nucleotide, along with deoxythymidine triphosphate (dTTP) and deoxyguanosine triphosphate (dGTP). After a 30-minute incubation period, the ability of telomerase to incorporate the nucleotide analogs into a telomere DNA product was evaluated by analyzing the extended products and comparing with those generated with dATP as the nucleotide substrate (**S1 Fig**). Extension of DNA products was negligible under these conditions, as product lengths were comparable to those measured in the complete absence of dATP and nucleotide analog (**S1 Fig**). These data suggest that telomerase cannot incorporate any of the analogs into telomere DNA products at the concentration tested or that selective incorporation of the indolyl analogs by telomerase causes chain termination to produce very short products.

Nucleotide 5-MeCITP inhibits telomerase activity in vitro

We next performed the direct in vitro telomerase activity assay in the presence of native deoxynucleoside triphosphates (dNTPs) along with each indolyl-2′-deoxynucleoside triphosphate analog. For initial experiments, native dATP concentrations were maintained near the predetermined relative rate constant ($K_{1/2}$) value of approximately 1 μM for the assay (**S2 Fig**) and in the presence of 200 μM nucleotide analog for a single reaction conducted at the pre-steady-state condition of 30 minutes (**S2 Fig and Fig 1B**). Extended products were analyzed to conclude that the addition of 6-nitroindolyl-2′-deoxyriboside 5′-triphosphate (6-NITP) resulted in a slight but significant ($p < 0.05$) decrease in telomerase activity (**Fig 1C**). Strikingly, 5-MeCITP produced a greater than 80% reduction in telomerase activity under identical conditions ($p < 0.0001$) (**Fig 1C**). None of the other analogs investigated behaved as inhibitors against telomerase activity under these experimental conditions, including 5-methylindolyl-2′-deoxyriboside 5′-triphosphate (5-MeITP) and 5-carboxylindolyl-2′-deoxyriboside 5′-triphosphate (5-CITP), which are structurally similar to 5-MeCITP (**Fig 1A and S1 Table**). These findings indicate that the combination of methyl and carboxyl moieties is required for effective inhibition of telomerase by 5-MeCITP.

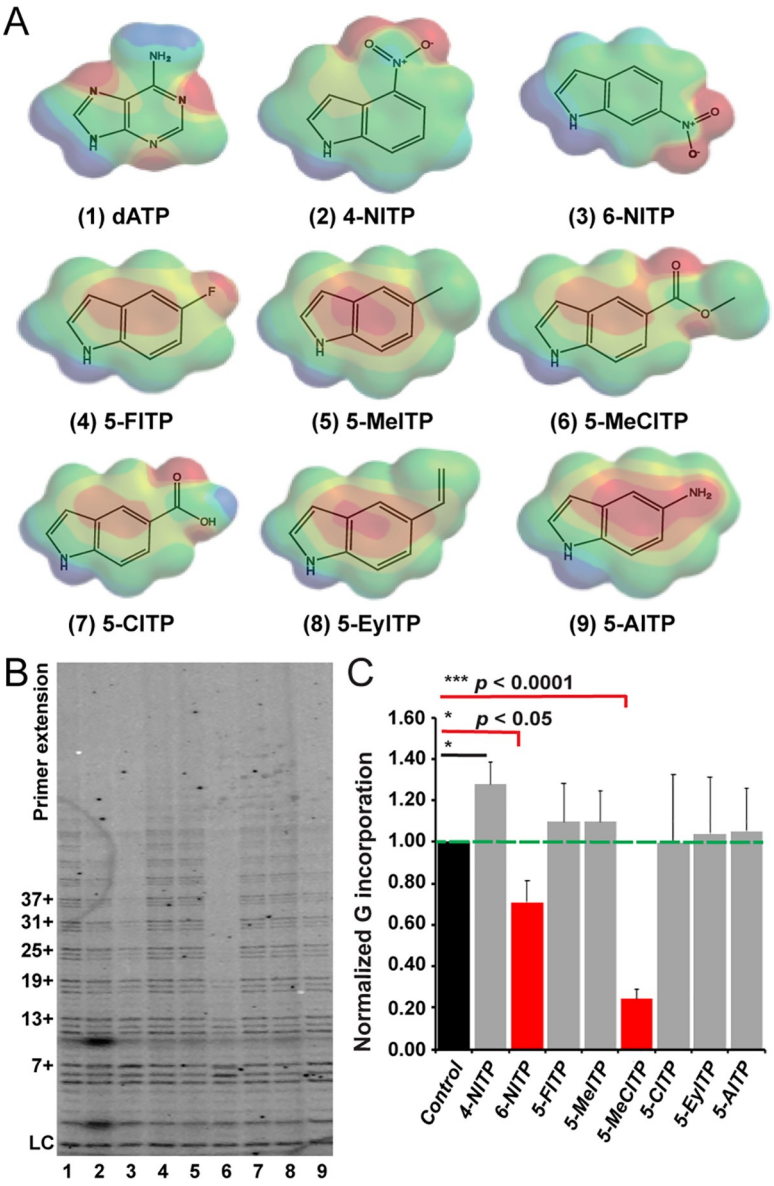

Fig 1. Nucleotide 5-MeCITP is an inhibitor of telomerase activity. (**A**) Chemical structures and electron density surface potentials of indolyl nucleotide analogs used in this study. For clarity, only nucleobase structures are shown. Abbreviations at the bottom of each nucleobase correspond to the full name of the nucleotide as described in S1 Table. (**B**) Screening of nucleotide analogs via the direct telomerase activity assay reveals that 5-MeCITP reduces telomerase activity by 80% compared with untreated control. Numbers at the bottom of the gel correspond to the analog number indicated in panel A. Control refers to untreated reaction. Values to the left of the gel depict the number of deoxynucleotides added by telomerase to the primer d(GGGTTA)$_3$. (**C**) Quantitation of G (dGTP) incorporation relative to control for samples analyzed in panel B. Error bars indicate the standard deviation calculated from three replicates. A two-tailed Student *t* test was used to determine *p*-values. $^{*}p < 0.05$, $^{***}p < 0.0001$. Data associated with this figure can be found in the supplemental data file (S1 Data). dATP, deoxyadenosine triphosphate; dGTP, deoxyguanosine triphosphate; LC, loading control; 5-MeITP, 5-methylindolyl-2′-deoxyriboside 5′-triphosphate; 4-NITP, 4-nitroindolyl-2′-deoxynucleoside 5′-triphosphate; 6-NITP, 6-nitroindolyl-2′-deoxynucleoside 5′-triphosphate; 5-AITP, 5-aminoindolyl-2′-deoxyriboside 5′-triphosphate; 5-CITP, 5-carboxylindolyl-2′-deoxyriboside 5′-triphosphate; 5-EyITP, 5-ethyleneindolyl-2′-deoxyriboside 5′-triphosphate; 5-MeCITP, 5-methylcarboxyl-indolyl-2′-deoxyriboside 5′-triphosphate.

https://doi.org/10.1371/journal.pbio.3000204.g001

To better define the impact of 5-MeCITP on telomerase activity, we compared its inhibitory effects with that of AZT triphosphate (AZT-TP). For these experiments, telomerase activity was measured in the presence of increasing inhibitor concentrations in a dose-dependent manner (Fig 2). The data were fit to calculate apparent rate constants ($K'_{1/2}$) for each compound that describes the concentration of inhibitor in which telomerase activity is 50% as compared with untreated controls. These constants were determined to be 118.89 ± 12.42 and 50.92 ± 9.79 μM for 5-MeCITP and AZT-TP, respectively, under these experimental conditions (Fig 2 and S3 Fig).

To probe the mode of binding of 5-MeCITP to telomerase, another experiment was performed using the direct telomerase assay in the presence of 400 μM 5-MeCITP and with increasing concentrations of dATP. Fitting of the data revealed a nearly complete recovery of telomerase activity at elevated concentrations of dATP (S4 Fig). The $K_{1/2}$ for dATP increased by approximately four times when the experiments were performed in the presence of 5-MeCITP (S4 Fig). Cumulatively, these results suggest that 5-MeCITP inhibits telomerase activity by competing with dATP binding.

The noncanonical binding of 5-MeCITP disturbs telomerase RNA template base positioning

To identify the precise interactions that govern 5-MeCITP binding to telomerase, we crystallized the *T. castaneum* TERT-MeCITP complex along with a nucleotide hairpin that functionally mimics the telomerase RNA template-telomere DNA substrate [18]. The structure of the complex refined to 2.8 Å identifies density corresponding to an unpolymerized 5-MeCITP residing in the active site of the enzyme (Fig 3 and S2 Table). The triphosphate group of 5-MeCITP is coordinated by two metal ions in a manner that is structurally similar to that of a nonhydrolyzable nucleotide analog bound to the active site of other polymerases [38–40]. The modified nucleobase of 5-MeCITP adopts a noncanonical configuration in which it is rotated 180˚ as compared with the expected orientation of a native dNTP forming Watson-Crick base pairs with the RNA template (S5 Fig). This configuration is very likely governed by an inability to properly base pair with RNA combined with selective interactions formed between the methylcarboxyl moiety of 5-MeCITP and TERT. Specifically, the methylcarboxyl moiety occupies a hydrophobic patch formed between motifs 1, 2 of the fingers domain and T-motif in the TRBD. The positioning of the methylcarboxyl group of 5-MeCITP is coordinated by interactions with Ile187 and Ile196 of motifs 1 and 2 and with Leu141 of the T-motif of *T. castaneum* TERT (Fig 3A–3C). The unique positioning of the modified nucleotide coincides with a displacement of the nucleobase of the template away from its canonical position (S5 Fig). It is worth noting that the RNA base displacement is likely to be subtle in the context of the full-length RNA, where additional protein-RNA contacts within telomerase stabilize this interaction [41]. Nonetheless, an overlay of the available TERT structures of *T. castaneum* [18], *Homo sapiens* [42], and *Tetrahymena thermophila* [43] highlights a structural arrangement that is relatively conserved among species (S6 Fig). Similarly, the interaction with the methylcarboxyl moiety of the artificial nucleotide in *T. castaneum* TERT is coordinated by two isoleucine residues located in motifs 1 and 2 that are conserved in the human enzyme (Fig 3D). The methylcarboxyl group of 5-MeCITP is coordinated by a leucine in *T. castaneum* and a phenylalanine in *H. sapiens*, residing in T-motif of TERT. While either amino acid would be expected to make similar hydrophobic contributions to the pocket that is formed, the presence of a bulkier phenylalanine in human TERT might provide a tighter pocket for 5-MeCITP to bind to or require a structural rearrangement to accommodate the methylcarboxyl moiety. In any event, an analogous hydrophobic pocket is very likely formed in human telomerase to trap 5-MeCITP in a similarly inactive state.

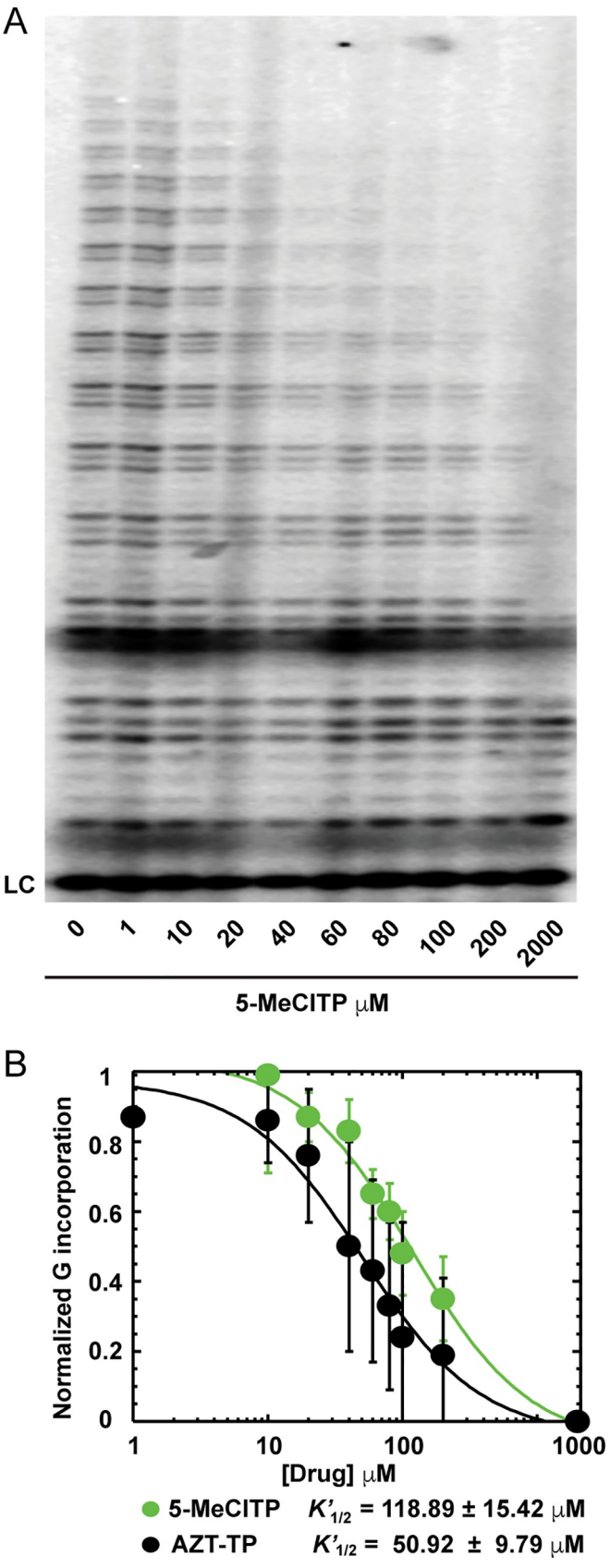
A
LC
0
1
10
20
40
60
80
100
200
2000
5-MeCITP μM
B
Normalized G incorporation
1
0.8
0.6
0.4
0.2
0
1
10
100
1000
[Drug] μM
5-MeCITP K'1/2 = 118.89 ± 15.42 μM
AZT-TP K'1/2 = 50.92 ± 9.79 μM

Fig 2. Nucleotides 5-MeCITP and AZT-TP inhibit telomerase in a dose-dependent manner. Direct telomerase extension assay with increasing concentrations of (**A**) 5-MeCITP (0–2 mM) and (**B**) AZT-TP (0–2 mM) reveal inhibition of telomerase activity in a dose-dependent manner. Activity (normalized G incorporation) was quantified and plotted against inhibitor concentration to determine relative $K'_{1/2}$ values for each compound ($n = 4$). Data associated with this figure can be found in the supplemental data file (S1 Data). AZT-TP, azidothymidine triphosphate; G, deoxyguanosine triphosphate; LC, loading control; 5-MeCITP, 5-methylcarboxyl-indolyl-2′-deoxyriboside 5′-triphosphate.

https://doi.org/10.1371/journal.pbio.3000204.g002

The co-crystal structure shows that 5-MeCITP does not form direct interactions with the RNA template, suggesting that inhibition is not specific to incorporation of a specific dNTP. Rather, 5-MeCITP likely prevents access of all dNTPs to the active site of telomerase. To test this hypothesis, we performed the direct telomerase incorporation assay with 5-MeCITP and human telomerase along with dATP, dTTP, or dGTP at limiting concentrations in the reaction. As anticipated, 5-MeCITP displayed similar inhibitory properties under all three conditions (S7 Fig). These results further suggest that the inhibition of telomerase by 5-MeCITP is not specific against a particular dNTP substrate, but that it competes with all dNTPs for access to the telomerase active site.

Nucleoside 5-MeCIdR leads to telomere shortening in a telomerase-dependent manner and is less toxic than AZT

We next characterized the growth properties of different cell lines that were treated with 5-MeCIdR, the cell-permeable nucleoside counterpart of 5-MeCITP. These studies used a panel of genetically distinct cell types that included A549 (lung cancer), HCT-116 (colon cancer), and MIA PaCa-2 (pancreatic cancer) cell lines that are telomerase positive, and U2OS (osteosarcoma) cells, which implement alternative lengthening of telomeres (ALT) instead of telomerase for maintaining telomere length. Finally, WI-38 (WI-38 VA13 subline) cells were used as human lung fibroblast cells that do not exhibit ALT or telomerase activity. In general, treatment with 5-MeCIdR (10–500 μM) for up to 3 days did not produce any adverse effects on cell viability for any of the five cell lines investigated (Fig 4A and 4B; S8 Fig). In contrast, AZT-treated cells exhibited lower cell survival in both telomerase-positive and telomerase-negative cell lines, especially at the elevated doses (>100 μM) (Fig 4A and 4B; S8 Fig).

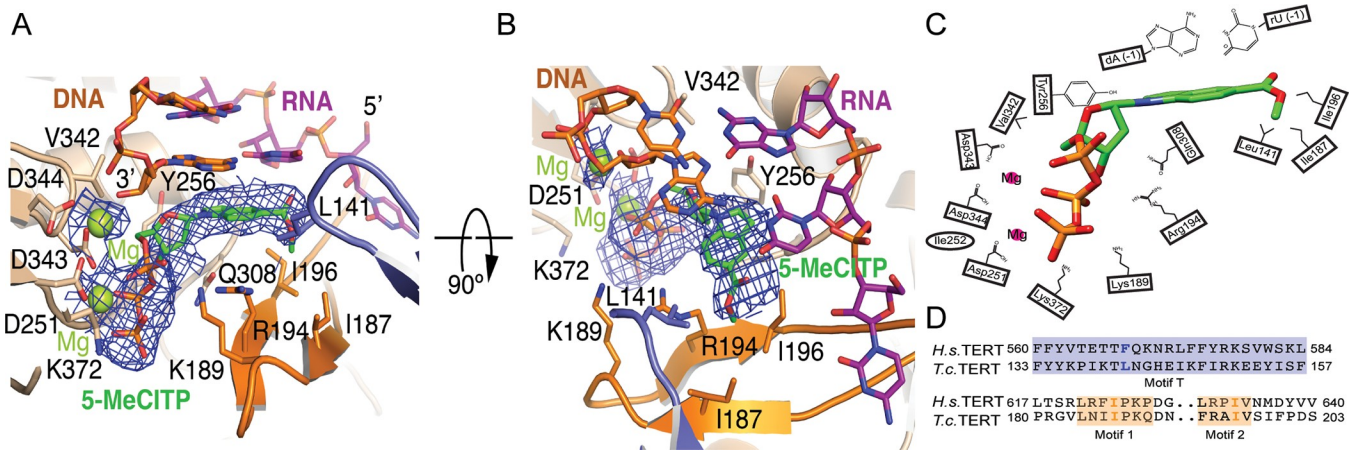

Fig 3. Nucleotide 5-MeCITP occupies the telomerase deoxynucleotide binding site and displaces the RNA template base. (**A**) Structure of *T. castaneum* TERT in complex with a hybrid RNA-DNA and 5-MeCITP. The RNA-binding domain is shown in blue, the finger domain in orange, and the palm domain in yellow. The RNA template strand is shown in purple and the DNA strand in orange. (**B**) Panel (A) rotated 90˚. (**C**) Two-dimensional diagram of the molecular interactions of 5-MeCITP with *T. castaneum* TERT. (**D**) Sequence alignment reveals sequence comparison of residues in the T-motif, and motifs 1 and 2 of *Homo sapiens* and *Tribolium castaneum* TERT. TERT, telomerase reverse transcriptase; 5-MeCITP, 5-methylcarboxyl-indolyl-2′-deoxyriboside 5′-triphosphate.

https://doi.org/10.1371/journal.pbio.3000204.g003

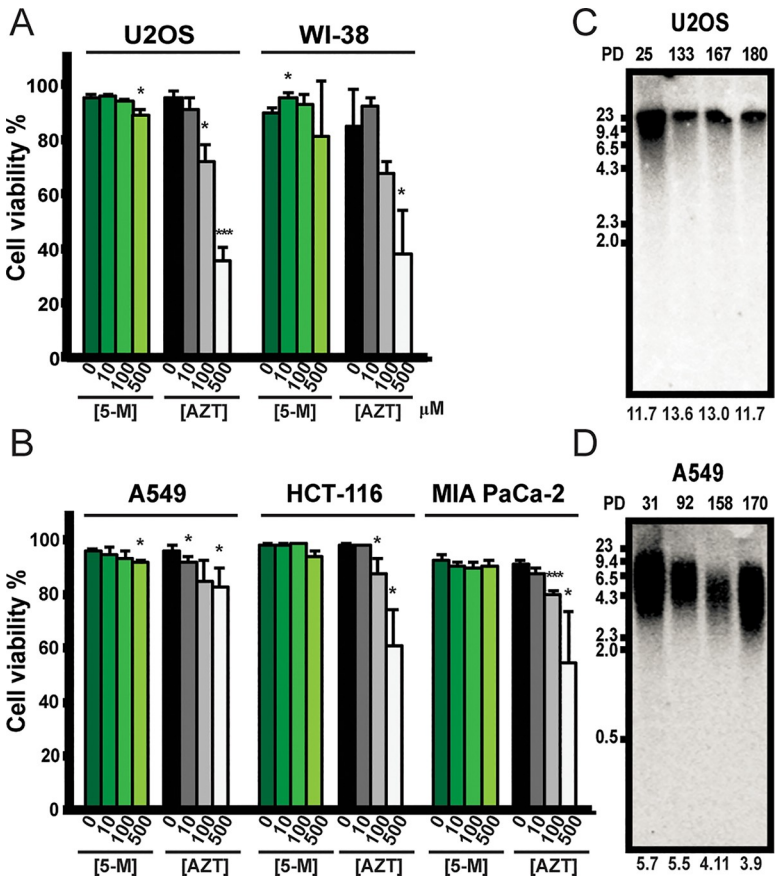

Fig 4. Nucleoside 5-MeCIdR leads to telomere shortening in telomerase-positive cells selectively. Trypan exclusion assay for telomerase-negative (**A**) and telomerase-positive cells (**B**) shows that 5-MeCIdR (abbreviated as 5-M, green scale bars) treatment is less toxic than AZT (gray scale bars) to all treated cells. $^{*}p < 0.05$, $^{***}p < 0.001$. Error bars indicate the standard deviation values from three replicate experiments. (**C**) Treatment of telomerase-negative U2OS cells with 100 μM 5-MeCIdR does not alter telomere length, while telomeres in telomerase-positive A549 cells (**D**) get shorter with increasing population doublings (PDs). Numbers at the bottom of the Southern blots indicate the average telomere lengths. Data associated with this figure can be found in the supplemental data file (S1 Data). AZT, azidothymidine; PD, population doubling; 5-M/5-MeCIdR, cell-permeable nucleoside form of 5-MeCITP.

https://doi.org/10.1371/journal.pbio.3000204.g004

We next monitored the effects of long-term exposure of cells to 5-MeCIdR (100 μM) on telomere length maintenance. Telomerase-negative U2OS cells treated with 5-MeCIdR maintained a constant telomere length distribution even after 180 population doublings (Fig 4C). In contrast, telomere length became progressively shorter in telomerase-positive A549, HeLa, and HCT116 cells treated with 5-MeCIdR and compared with DMSO control (Fig 4D and S9 Fig). Consistent with these data, long-term administration of 5-MeCIdR resulted in a significant increase in senescence-associated β-galactosidase activity in telomerase-positive cancer cells as compared with DMSO-treated control cells (S10 Fig). In summary, these data indicate that 5-MeCIdR treatment selectively leads to telomere shortening and initiates senescence in telomerase-positive cancer cells.

Discussion

As most tumors rely on telomerase to drive cellular immortality, the development of compounds designed to selectively impede telomerase activity remains a promising therapeutic strategy. In this study, we tested the ability of a set of indolyl nucleotide analogs that display

diverse physicochemical properties to impede telomerase function. These results, and especially the identification of 5-MeCITP as an inhibitor of telomerase, provide exciting potential for further drug development.

While used with other antiviral agents in the treatment of HIV-1, the administration of AZT is associated with enhanced cytotoxicity in healthy cells, which has limited its clinical potential [44–48]. Here, we report that 5-MeCITP inhibits telomerase activity with a potency similar to that of AZT-TP. Compared with AZT, however, 5-MeCIdR administration was more tolerated by cells and produced minimal changes in cell viability. Together, these data indicate that 5-MeCIdR treatment is generally more tolerated by cells than AZT, potentially due to higher selectivity that limits off-target effects on metabolic pathways and non-telomerase polymerases.

Our results also provide essential and fundamental knowledge regarding the selectivity of small-molecule interactions with the telomerase catalytic site. For example, the structure of 5-MeCITP bound to *T. castaneum* TERT reveals that the carboxyl group helps to position the methyl moiety at a distance away from the ribose ring so that the methyl can fit into a specific hydrophobic pocket of TERT, while the phosphate groups and ribose ring occupy a native-like position in the active site of the enzyme. This finding could explain why the active site of telomerase is more selective for 5-MeCITP over the other nucleotide analogs we investigated, a notion that is supported by docking experiments. In this set of experiments, none of the other analogs were predicted to bind in a manner such that the modifications within the nucleobase could access the hydrophobic pocket formed by the T-motif and motifs 1 and 2 while concomitantly occupying the nucleotide binding pocket of TERT (**S11 Fig**). As such, it is very likely that the carboxyl group of 5-MeCITP merely serves as an extension to place the aliphatic methyl moiety in the vicinity of the hydrophobic pocket of TERT so that it may form favorable interactions there.

As the specific, physicochemical properties of 5-MeCITP facilitate its interactions with telomerase, the elements that form the unique binding pocket of telomerase might similarly explain the selective nature of 5-MeCITP binding to telomerase over other polymerases. Interestingly, the hydrophobic binding pocket of telomerase is formed by regions that are specific to telomerase (**S12 Fig**). The T-motif is a conserved structure that is unique to TERT proteins. It is postulated to interact with the template boundary element (TBE) [41] located just upstream of the RNA template to help mediate positioning of the RNA template to guide nucleotide selection and facilitate telomerase processivity [49–51]. Motifs 1 and 2 form an insertion within the fingers subdomain and are conserved among the RT family, including TERTs [7,29]. Interestingly, 5-MeCITP also inhibits HIV-1 RT activity [32]. Therefore, it is predicted that motifs 1 and 2 provide the more favorable interactions to promote 5-MeCITP binding to HIV-1 RT or TERT active sites and that contributions from the TERT-specific T-motif play a less prominent role in the selective binding of this analog. In contrast to HIV-1 RT and TERT enzymes, other DNA polymerases lack the analogous environment formed by motifs 1 and 2 in the active site and coincidentally lack the putative hydrophobic pocket that facilitates interactions of 5-MeCITP with telomerase (**S12 Fig**). As a result, 5-MeCITP does not inhibit DNA polymerases such as T4 DNA polymerase and *E. coli* Klenow fragment. Instead, these polymerases can effectively incorporate 5-MeCITP, at least at positions that are opposite abasic sites in the template DNA [32,36].

The X-ray crystal structure of *T. castaneum* TERT bound with an RNA template mimic and a complementary telomeric single stranded DNA (ssDNA) has a 3′ deoxyguanosine (dG) nucleotide occupying the catalytic site [18]. That particular structure represents a post-polymerization state in which the terminal dG is covalently bound to the synthesized ssDNA and its lone backbone phosphate group is coordinated by a single Mg^{2+} ion. In contrast, the

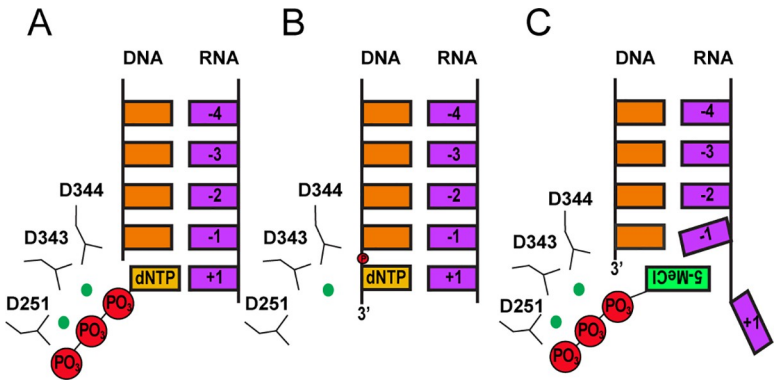

Fig 5. Proposed mechanism of action of 5-MeCITP for inhibiting telomerase activity. (**A**) Pre-polymerization state of a natural telomerase substrate (dNTP). The two magnesium ions help to coordinate the nucleophilic attack of the 3′-OH of the terminal dNTP of the telomeric DNA strand on the α-phosphate group of the dNTP in the TERT active site. (**B**) Post-polymerization state of a natural telomerase dNTP substrate. The dNTP forms a Watson-Crick base pair with the RNA template to aid in nucleophilic attack of the phosphate backbone for incorporation into the synthesized DNA strand. (**C**) 5-MeCITP does not base pair appropriately with the RNA template, thereby occluding the RNA from the active site. As a consequence, 5-MeCITP is not incorporated into the DNA chain. dNTP, deoxynucleotide triphosphate; TERT, telomerase reverse transcriptase; 5-MeCITP, 5-methylcarboxyl-indolyl-2′-deoxyriboside 5′-triphosphate.

https://doi.org/10.1371/journal.pbio.3000204.g005

structure presented here reveals that 5-MeCITP is not incorporated into the DNA strand and instead binds to the *T. castaneum* TERT active site with the triphosphate coordinated by a pair of Mg^{2+} ions (Fig 3). The α-phosphate of 5-MeCITP is situated at a distance that is approximately 5 Å from the nucleophilic 3′-hydroxyl group of the terminal dATP of the ssDNA that is being extended and is therefore too far for nucleophilic attack and incorporation into the 3′ end of the DNA. Additionally, the inability of 5-MeCITP to properly base pair with the RNA template most likely prevents the nucleotide analog from adopting a position that would facilitate polymerization into the ssDNA chain. Without base pairing, the nucleobase of 5-MeCITP forms alternative interactions in the TERT active site. Specifically, our data reveal that it flips so that the methylcarboxyl group can selectively form hydrophobic interactions with the unique pocket formed by the T-motif and motifs 1 and 2 of TERT. This unorthodox positioning in the TERT active site further perturbs the complementary RNA base away from the active site (Fig 5). In summary, the inability of the modified nucleotide to form proper Watson-Crick base pairs with RNA combined with the favorable and unique interactions formed with TERT are important contributors to 5-MeCITP's unique mechanism of action. The structure-function studies reported here therefore provide an opportunity to develop additional analogs to exploit these properties and to develop more selective and potent telomerase inhibitors.

Methods

Nucleotide analogs

Nucleotide analogs 4-NITP [33], 6-NITP [33], 5-FITP [34], 5-MeITP [35], 5-MeCITP [36], 5-CITP [32], 5-EyITP [35], and 5-AITP [34] were characterized and synthesized as previously described. AZT-TP was purchased from Trilink Biotechnologies.

Direct telomerase incorporation assay

Telomerase activity assays were performed as described previously [37]. Briefly, 2 μL of hTR and hTERT-transfected HEK 293T cell lysate (super telomerase cell extracts) were used in each 20-μL reaction. Unless otherwise noted, all assays were conducted with a mixture

containing 35 mM Tris-HCl, pH 8.0, 0.7 mM $MgCl_2$, 1.8 mM β-mercaptoethanol, 0.7 mM spermidine, 35 mM NaCl, 100 μM dTTP, 100 μM dATP, 2.9 μM dGTP, 0.33 μM [α-^{32}P]-dGTP (10 μCi/μL, 3000 Ci/mmol, Perkin–Elmer), and 1 μM 18-nt substrate $d(GGGTTA)_3$ primer. Each reaction was carried out for 30 minutes at 30˚C before quenching with 100 μL of a quench buffer containing 3.6 M NH_4OAc, 300 μM glycogen, and 400 μM EDTA. In each reaction, a 5′-^{32}P–labeled hT18 primer $(GGGTTA)_3$ was used as a loading control. All ssDNA products were ethanol precipitated and analyzed on a 12% polyacrylamide/7 M urea/1X Tris-Borate-EDTA denaturing gel. The gels were dried and exposed overnight to phosphorimager plates, which were imaged on a Typhoon FLA 9500 bimolecular imager (GE Healthcare), and densitometry was performed by SAFA footprinting software [52]. Quantification of telomerase assay products (normalized G incorporation) were used to determine total enzyme activity for each reaction by quantifying the signal of all dGTPs incorporated into the extended products, according to Eq 1.

$$G\ incorporation = \sum \frac{Norm.R_f * Reference\ LC}{LC\ of\ the\ lane} \quad (1)$$

where *Norm. R_f* refers to the normalization of the radioactivity factor and is obtained by dividing the raw intensity values by the number of Gs added to the extended primer. LC of the lane refers to loading control for each individual lane, while Reference LC refers to a common loading control used for normalization between lanes. Dose response curves were generated by plotting the G incorporation value against the concentration of the drug being added.

Direct telomerase incorporation assay to determine $K_{1/2}$

The $K_{1/2}$ determination for each dNTP was conducted under the standard telomerase extension assay conditions described in the direct telomerase incorporation assay in the Methods section, but with increasing concentrations of that particular dNTP that ranged from 0–100 μM. Normalized G incorporation was plotted against that dNTP concentration. Normalized G incorporation was calculated by following Eq 1, and each reaction was then normalized as indicated in each figure. Normalized G incorporation was plotted against deoxynucleotide (dATP or dTTP) concentration to generate a dose-response curve that was fit by a hyperbolic equation using Kintek Explorer 7.6 software [53] and KaleidaGraph.version 3.5. The hyperbolic equation used to fit the data is described in Eq 2:

$$Normalized\ G\ incorporation = a * \frac{[dNTP]}{K_{1/2} + [dNTP]} + c \quad (2)$$

where *a* is the amplitude, *c* is the offset, and [*dNTP*] is the deoxynucleotide triphosphate concentration that is changing (dATP or dTTP).

For the experiments of substrate competition between dATP and 5-MeCITP, the telomerase assay was performed with 400 μM 5-MeCITP and increasing concentrations of dATP that ranged from 0 to 100 μM. The quantitation and fitting of this data was done as explained above using Eqs 1 and 2. To determine whether 5-MeCITP blocked incorporation of dTTP, dATP, or dGTP, the telomerase assay was performed under standard conditions with differing dNTP concentrations. To determine whether 5-MeCITP blocked incorporation of dTTP, the dNTP concentrations were 3 μM dGTP (including 10% [α-^{32}P]-dGTP), 2 μM dTTP, 100 μM dATP, and 0 to 400 μM 5-MeCITP. To determine whether 5-MeCITP blocked incorporation of dGTP, the dNTP concentrations were 3 μM dGTP, 2 μM dTTP that included 2 μL [α-^{32}P]-dTTP (10 μCi/μL, 3000 Ci/mmol, Perkin–Elmer), 100 μM dATP, and 0 to 400 μM 5-MeCITP.

Direct telomerase incorporation assay to determine $K'_{1/2}$ of AZT and 5-MeCITP

For assays involving 5-MeCITP, concentrations of dTTP were maintained at 100 μM and dATP at a concentration near its determined $K_{1/2}$ value of 1 μM, along with increasing concentrations of 5-MeCITP that ranged from 0 to 2 mM. The observed $K'_{1/2}$ of AZT-TP was determined in a similar manner but with dTTP used at a limiting concentration near its $K_{1/2}$ value of 2 μM and dATP at 100 μM. For these reactions, increasing concentrations of AZT-TP (0–2 mM) were added to each reaction at the specified dose. Normalized G incorporation was calculated following Eq 1, and each reaction was then normalized to the reaction with no inhibitor or as indicated in each figure. Normalized G incorporation was plotted against inhibitor concentration to generate a dose-response curve that was fit by a hyperbolic equation using Kintek Explorer 7.6 software [53] and KaleidaGraph.version 3.5. The hyperbolic equation used to fit the data is described in Eq 3:

$$Normalized\ G\ incorporation = a * \frac{[i]}{K'_{1/2} + [i]} + c \quad (3)$$

where a is the amplitude, c is the offset, and $[i]$ is the inhibitor concentration. This fitting generated an observed affinity constant rate value ($K'_{1/2}$) that describes the inhibitor concentration needed to observe half of the normalized G incorporation.

Cell culture

Human HCT116, MIA PaCa-2, A549, HeLa, WI-38, and U2OS cell lines were obtained from ATCC. All cell lines were grown in Dulbecco's Modified Eagle Medium (DMEM) supplemented with 10% fetal bovine serum (FBS) at 37˚C with 5% CO_2. For viability studies, cells were treated with a final concentration of 100 μM 5-MeCIdn in the presence of 0.0003% DMSO or with 0.0003% DMSO alone. Every 4 days cells were provided fresh media containing analog/DMSO or DMSO alone. Every 7 days, cells were counted, and 5.0×10^4 cells were transferred into a new plate with fresh media containing nucleotide analog/DMSO or DMSO. For generation of growth curves, the cells were treated with the indicated drugs for 5 days and trypsinized. Viable cells were identified by trypan blue exclusion and counted on a hemocytometer.

Telomere restriction fragment analysis

Telomere restriction fragment (TRF) analysis was performed using a commercial kit using standard protocols (TeloTAGGG Telomere Length Assay, Catalog no. 12209136001, Roche Diagnostics Corporation, Indianapolis, IN). DNA was extracted from A459, HCT116, MIA-Pa-Ca-2, Wi-38, and U2OS cells after 6 months' treatment with 100 μM of 5-MeCIdR/DMSO or DMSO alone. A total of 2 μg DNA was digested overnight with Rsa I and Hinf I at 37˚C and electrophoresed through 0.8% agarose gels in 1 × TAE at 50 V for 4 hours. Gels were denatured and neutralized prior to capillary transfer overnight. Telomeric DNA was transferred onto a Hybond-N^+ membrane (GE Healthcare, Chicago, IL) using 20× SSC buffer. The transferred DNA was fixed by UV cross-linking. The cross-linked membrane was then hybridized with a ^{32}P-labeled synthetic telomere probe with the sequence $(GGGTTA)_4$ overnight at 42 ˚C. After hybridization, the membrane was washed with buffer 1 (2× SSC, 0.1% SDS) at room temperature for 15 minutes and then washed twice with buffer 2 (0.5× SSC, 0.1% SDS) at 55 ˚C for 15 minutes. The membranes were exposed overnight to phosphorimager plates, which were imaged on a Typhoon FLA 9500 biomolecular imager (GE Healthcare, Chicago,

IL). Image quantification was performed using ImageQuant software to measure the intensity value of each telomere smear. The weighted centers of mass of density plot profiles were generated for each sample. Numeric values generated from the histograms were compared against values of a known molecular weight standard, to obtain the average telomere length.

Telomere quantitative fluorescence in situ hybridization

HeLa and HCT116 cells were plated (200,000 cells/well in six-well plate) directly on coverslips. Cells were fixed with 4% paraformaldehyde, permeabilized with 0.5% Triton X-100, and dehydrated through graded alcohols prior to hybridization with a fluorescently labeled telomere leading strand PNA probe [5′-$(CCCTAA)_3$–3′] (Cy5-TelC; PNA Bio, Newbury Park, CA) overnight at 25˚C in a humidified chamber. Cells were washed twice with PNA wash buffer (70% formamide, 10 mM Tris-HCl pH 7.5, 1% BSA), counterstained with DAPI (1 μg/mL in PBS), and mounted onto glass slides with Fluoromount-G (Thermo Fisher Scientific, Waltham, MA). Images were captured using a Leica TCS SP8 STED confocal microscope (Light Microscopy Imaging Core, CWRU) and analyzed using the Leica Application Suite X (LAS X).

Colony forming assay

Cells were treated with vehicle, AZT, or 5-MeCIdn for 3 days and then harvested. For each treatment group, 500 viable cells (HCT116, A549, U2OS, or WI-38) were seeded in three 35-mm plates and evenly dispersed. The cells were then grown in drug-free media for 11 days. The colonies were fixed (75% methanol and 25% acetic acid) for 15 minutes at room temperature and stained (0.05% crystal violet and 95.05% methanol) for 30 minutes at room temperature.

Senescence-associated β-galactosidase staining

Cultured cells were plated into six-well dishes with a cover glass on it one week before staining. Cover glasses were collected and cells on it were fixed and stained as per the manufacturer's protocol (Senescence β-Galactosidase Staining Kit, Cell Signaling Technology no. 9860, Danvers, MA). Stained cells were imaged with a Leica SCN400 slide scanner. Ten random images were collected and cells counted with ImageJ 1.52e software. Staining was conducted 5 months after continual treatment with 100 μM 5-MeCIdR/DMSO or DMSO alone.

Protein crystallization and data collection

The *T. castaneum* TERT protein was purified as described by Mitchel and colleagues [18]. The protein was dialyzed in 10 mM Tris-HCl, 100 mM KCl, 1 mM TCEP, pH 7.5 prior to crystallization trials. The ternary complex was prepared by adding to the 10 mg/mL dialyzed protein, 1.2 molar excess nucleic acid consisting of the putative RNA template and the complementary telomeric DNA (rCrUrGrArCrCrUrGrArCTTCGGTCAGGTCA—Integrated DNA Technologies), 1 mM 5-MeCITP, and 2.5 mM $MgCl_2$. Crystals of the monoclinic space group $P2_1$ were grown by the vapor diffusion sitting drop method. Drops were prepared by mixing one volume of the ternary complex with one volume of reservoir solution containing 0.1 M HEPES (pH 7.5), 8% PEG 8K, and 0.1 M KCl. The crystals were transferred into a cryosolution containing 0.1 M HEPES (pH 7.5), 8% PEG 8K, 30% PEG400, 0.1 M KCl, and 1 mM TCEP and flash frozen in liquid nitrogen. Data were collected from three crystals on a Rigaku MicroMax-007 HF rotating anode X-ray generator (wavelength 1.54178 Å) with VariMax optics and using a Saturn 944 HG CCD detector. The crystals were kept frozen with an Oxford Cryosystems Cobra system at 100 K during the data collection. The data were processed and scaled with XDS [54]

(S2 Table). The coordinates and structure factors of the *T. castaneum* TERT-5-MeCITP complex have been deposited in the Protein Data Bank (PDB ID: 6E53).

Structure determination and refinement

Phases were calculated by molecular replacement (MR) using PHASER [55] as implemented in PHENIX [56] using the *T. castaneum* TERT-hybrid structure (PDB ID: 3KYL) as a search model. The maps revealed clear *fo-fc* density for 5-MeCITP at 3.0 sigma contour level bound at the active site of the enzyme. Model building was carried out in COOT [57] and the model was refined using REFMAC5 [58] (S2 Table). The structure was refined to good stereochemistry with 92.1% and 7.9% of the residues in the "most favorable" and "additional allowed" of the Ramachandran plot, respectively.

Molecular modeling and docking

T. castaneum TERT, HIV-1 RT, and Klenow fragment polymerase were loaded into Maestro (Schrodinger 2017–3 suite) using their PDB ID *(T. castaneum* TERT PDB ID: 3KYL; HIV-1 RT PDB ID: 3V4I; Klenow fragment polymerase PDB ID: 1KFD). Models were subjected to the Protein Preparation protocol with Workspace Structure Preprocessing, H-bond Assignment, and Restrained Minimization at default settings. Binding sites were defined by using the Receptor Grid Generation protocol, at default settings. dATP and other nucleoside analogues were modeled in with the software and docked at the respective binding sites using the Ligand Docking protocol, which allows for flexible docking using Extra Precision (XP) settings while also restricting docking to a reference position with tolerance of 0.10 Å. Reference position was designated as the location of ligand contained in their respective PDB files.

Statistical analysis

All statistical analyses were carried out using Excel software. Unless otherwise noted, experiments were conducted in triplicate. Comparisons between groups were performed using two-tailed Student *t* test. Statistical significance was considered if *p*-values were <0.05. Individual *p*-values are indicated in figure legends. All results are expressed as means ± SD.

Supporting information

S1 Table. Physiochemical properties of indoly-2′-deoxynucleotide analogs used in this study.
(DOCX)

S2 Table. X-ray crystallography data collection and refinement statistics.
(DOCX)

S1 Fig. Artificial indolyl nucleotide analogs are not incorporated by telomerase into extended DNA products in vitro. The in vitro direct telomerase extension assay was performed to determine whether any of the nucleotide analogs could replace native dATP for telomerase-mediated extension of telomere DNA. Values on the left of the assay depict the number of nucleotides added by telomerase to a telomeric-mimic primer d$(GGGTTA)_3$. The labels at the top define the nucleotide, either dATP or the artificial analog, that was used along with dTTP and dGTP for telomere extension in the reaction. dATP, deoxyadenosine triphosphate; dGTP, deoxyguanosine triphosphate; dTTP, deoxythymidine triphosphate; LC, loading control.
(TIF)

S2 Fig. Determination of $K_{1/2}$ for dATP and dTTP in the telomerase extension assay. (**A**) Telomerase activity assay (top) in the presence of increasing concentrations of dATP (0, 0.1, 0.2, 0.3, 0.4, 0.5, 0.6, 0.7, 0.8, 0.9, 1, 5, and 10 μM) was fitted with a hyperbolic equation (bottom) to determine observed $K_{1/2}$ value of dATP ($n = 4$). (**B**) Telomerase activity assay (top) in the presence of increasing concentrations of dTTP (0, 0.5, 1, 1.5, 2, 3, 3.5, 5, 10, and 100 μM) was fitted with a hyperbolic equation (bottom) to determine observed $K_{1/2}$ value of dTTP ($n = 4$). (**C**) Telomerase activity assay reveals that increased extension times (0–120 mins) correlate with increased product. The red asterisk at 30 minutes indicates the pre-steady-state time point that was chosen for subsequent in vitro telomerase activity assays. dATP, deoxyadenosine triphosphate; dTTP, deoxythymidine triphosphate.
(TIF)

S3 Fig. Inhibition of telomerase by AZT-TP. (**A**) An in vitro telomerase activity assay was performed with increasing concentrations of AZT-TP to calculate the $K'_{1/2}$ under these experimental conditions and for comparison to that of 5-MeCITP. (**B**) AZT chemical structure and electron density of nucleobase surface potentials. For clarity, the triphosphate group was not included in the structure. AZT, azidothymidine; AZT-TP, AZT triphosphate; 5-MeCITP, 5-methylcarboxyl-indolyl-2′-deoxyriboside 5′-triphosphate.
(TIF)

S4 Fig. Nucleotide 5-MeCITP competes with dATP in telomerase extension assays. (**A**) Direct telomerase extension assay with increasing concentrations of dATP (0, 0.2, 0.4, 0.8, 1, 4, 10, and 100 μM) in the absence (control, left side) and in the presence of 5-MeCITP (400 uM) (right side). (**B**) Quantification and hyperbolic fitting generated from the normalized G (dGTP) incorporation in the absence or presence of 5-MeCITP shown in panel A, with their respective $K_{1/2}$ determined in the absence (black) or presence (green) of 5-MeCITP. Data associated with this figure can be found in the supplemental data file (S1 Data). dATP, deoxyadenosine triphosphate; dGTP, deoxyguanosine triphosphate; 5-MeCITP, 5-methylcarboxyl-indolyl-2′-deoxyriboside 5′-triphosphate.
(TIF)

S5 Fig. The nucleobase of 5-MeCITP adopts a distinct binding mode compared with native dATP. (**A**) Overlay of 5-MeCITP bound (yellow) and dATP bound (blue) structures highlights differences in the binding pocket induced by the binding of 5-MeCITP (green) versus native dATP (blue). (**B**) Panel A rotated 90˚. (**C**) View perpendicular to the nucleobase of superposed cognate dATP (blue) and 5-MeCITP (green). The superposition reveals that 5-MeCITP adopts an orientation in the TERT binding site, where the nucleobase is flipped 180˚ compared with that of dATP. dATP, deoxyadenosine triphosphate; TERT, telomerase reverse transcriptase; 5-MeCITP, 5-methylcarboxyl-indolyl-2′-deoxyriboside 5′-triphosphate.
(TIF)

S6 Fig. Overlay of *Tribolium castaneum* TERT-RNA-DNA complex, *Homo sapiens* TERT, and *Tetrahymena thermophila* TERT shows structural conservation. (**A**) Overlay of *T. castaneum* TERT-RNA-DNA complex (green; PDB ID 3KYL), *H. sapiens* TERT (yellow; constructed by fitting of *T.t* TEN domain (PDB ID 2B2A) and *T.c* TERT, as independent domains, (PDB ID 3KYL) into the *H.s* telomerase cryo-EM map (EMD 7518)) and *T. thermophila* TERT (salmon; PDB ID 6D6V). The overlay indicates a conserved mechanism of RNA template and telomeric DNA binding. It is worth noting that in the *T. castaneum* TERT complex, several nucleotides at the 5′ end of the DNA and 3′ end of the RNA were introduced for crystallographic purposes and that portions of the nucleic acid do not make contacts with TERT. (**B**) Zoomed-in representation of panel A focused at the 3′ end of the telomeric DNA

and where the 5-MeCITP binds. This view shows a high degree of conservation within this telomerase region across these three species. (**C**) Overlay of *T*. *castaneum* TERT-RNA-DNA complex (green) and *T*. *thermophila* TERT (salmon) active site. The main difference is that the loop K_{481}HKEGS_{486} (*Tetrahymena* numbering; highlighted in red) in the RNA binding domain of the *T*. *thermophila* TERT structure includes more polar residues and is slightly displaced from the RNA template. EM, electron microscopy; TERT, telomerase reverse transcriptase; 5-MeCITP, 5-methylcarboxyl-indolyl-2′-deoxyriboside 5′-triphosphate.
(TIFF)

S7 Fig. Nucleotide 5-MeCITP competes with native dNTPs to inhibit telomerase activity. Direct in vitro telomerase assay was performed with limiting concentrations of (**A**) dTTP, (**B**) dGTP, or (**C**) dATP and with increasing concentrations of 5-MeCITP. For each experiment, the identified native nucleotide was maintained at a limiting concentration near its calculated $K_{1/2}$ value. Under each condition, telomerase activity was consistently inhibited with increasing 5-MeCITP concentrations. dATP, deoxyadenosine triphosphate; dGTP, deoxyguanosine triphosphate; dNTP, deoxynucleotide triphosphate; dTTP, deoxythymidine triphosphate; 5-MeCITP, 5-methylcarboxyl-indolyl-2′-deoxyriboside 5′-triphosphate.
(TIF)

S8 Fig. Nucleotide 5-MeCIdR versus AZT treatment in telomerase-positive and -negative cell lines. Colony assay formation of (**A**) MIA-Pa-Ca-2 (telomerase positive), (**B**) HCT116 (telomerase positive), and (**C**) U2OS (telomerase negative) after 5 days of treatment reveals that AZT is associated with significantly reduced cell survival as compared with 5-MeCIdR. $N = 3$. Error bars indicate the standard deviation values of three replicates. Two-tailed Student *t* test, $^{*}p < 0.05$, $^{**}p < 0.005$. Data associated with this figure can be found in the supplemental data file (S1 Data). AZT, azidothymidine; 5-MeCIdR, cell-permeable nucleoside form of 5-MeCITP.
(TIF)

S9 Fig. Nucleoside 5-MeCIdR leads to telomere shortening in telomerase-positive cells. Telomere length after 1 month's treatment of 100 μM 5-MeCIdR in telomerase-positive HeLa cells (**A**) gets shorter with increasing PDs, while mock treated HeLa cells' telomeres get longer over time. Numbers at the bottom of the Southern blots indicate the average telomere lengths. (**B**) Q-FISH shows higher fluorescent intensity for (**B**) HCT116 and (**C**) HeLa at Passage 1 (P1). Following treatment with 100 μM 5-MeCIdR (5-month HCT116, 1-month HeLa), telomere fluorescent intensity is considerably decreased when compared with mock induced conditions. Data associated with this figure can be found in the supplemental data file (S1 Data). PD, population doubling; Q-FISH, quantitative fluorescence in situ hybridization; 5-MeCIdR, cell-permeable form of 5-MeCITP.
(TIF)

S10 Fig. Nucleoside 5-MeCIdR induces senescence in telomerase-positive cells A549, MIA-Pa-Ca-2, and HCT116. SA-β-gal, a senescence marker, was used for staining of telomerase-positive cells A549 MIA-Pa-Ca-2 and HCT116 after treatment with 100 μM 5-MeCIdR or DMSO (control) for 5 months. (**A**) Photographic images (magnification 20×) and (**B**) quantitation of the data. $^{**}p < 0.005$, $^{***}p < 0.0001$. Data associated with this figure can be found in the supplemental data file (S1 Data). 5-MeCIdR, cell-permeable nucleoside form of 5-MeCITP.
(TIFF)

S11 Fig. Predictive models of interactions of the non-native nucleotide analogs docked into the *Tribolium castaneum* TERT structure. In silico models of dATP and nucleoside analogs (**A**. dATP, **B**. 6-NITP, **C**. 5-MeITP, **D**. 5-MeCITP, **E**. 5-FITP, **F**. 5-EyITP, **G**. 5-CITP, **H**. 5-AITP, **I**. 4-NITP) docked into the binding site of the *T*. *castaneum* TERT structure. Models were generated with Maestro (Schrodinger 2017–3) using Ligand Docking in the *T*. *castaneum* TERT structure; PDB ID: 3KYL. Generated models predict that the side chain of 5-MeCITP exclusively forms favorable interactions with a hydrophobic pocket of TERT that is formed by the unique motifs 1 and 2 and motif T of TERT proteins. dATP, deoxyadenosine triphosphate; TERT, telomerase reverse transcriptase; 4-NITP, 4-nitroindolyl-2′-deoxynucleoside 5′-triphosphate; 6-NITP, 6-nitroindolyl-2′-deoxynucleoside 5′-triphosphate; 5-AITP, 5-aminoindolyl-2′-deoxyriboside 5′-triphosphate; 5-CITP, 5-carboxylindolyl-2′-deoxyriboside 5′-triphosphate; 5-EyITP, 5-ethyleneindolyl-2′-deoxyriboside 5′-triphosphate; 5-FITP, 5-fluoroindolyl-2′-deoxyriboside 5′-triphosphate; 5-MeCITP, 5-methylcarboxyl-indolyl-2′-deoxyriboside 5′-triphosphate; 5-MeITP, 5-methylindolyl-2′-deoxyriboside 5′-triphosphate.
(TIFF)

S12 Fig. Interactions of 5-MeCITP with *Tc*TERT compared with predicted interactions of 5-MeCITP with HIV-RT and *Escherichia coli* Klenow fragment DNA polymerase I. Comparison of 5-MeCITP in the binding site of *T*. *castaneum* TERT (**A**), HIV-RT (**B**), and Klenow fragment DNA polymerase I (**C**). The overall conserved domains of the polymerases' structures are depicted, with the finger domain shown in orange, the palm domain colored yellow, and the thumb domain in red. The TERT-specific TRBD is covered blue in panel A. The RT/TERT-specific motif 1 and motif 2 are identified at the bottom as 1 and 2 in orange, respectively, in panels A and B. The TERT-specific motif T is identified as T with blue borders in panel A. At the top of each panel, the domain organization of *T*. *castaneum* TERT, HIV-RT, and Klenow fragment DNA polymerase I are shown color coded as previously stated. In the middle row, the ribbon representation of the three-dimensional structures of each polymerase with 5-MeCITP modeled into the active site is shown. In the bottom row, a close-up view of the modeled 5-MeCITP is shown along with the surface area of the active site for each polymerase. Docking of 5-MeCITP, and binding site surface, were created in Maestro (Schrodinger 2017–3). HIV-RT, human immunodeficiency virus reverse transcriptase; *Tc*TERT, *T*. *castaneum* telomerase reverse transcriptase; TERT, telomerase reverse transcriptase; TRBD, telomerase RNA-binding domain; 5-MeCITP, 5-methylcarboxyl-indolyl-2′-deoxyriboside 5′-triphosphate.
(TIF)

S1 Data. Data.
(XLSX)

Acknowledgments

We would like to thank Dr. Michael Harris, Dr. Eckhard Jankowsky, and Armend Axhemi for helpful discussions regarding the design of several experimental procedures. We acknowledge Dr. Franklin Mayca-Pozo and the CWRU SOM Light Microscopy Core Facility for assistance with the senescence assay. We would also like to thank Dr. Joachim Lingner for generously sharing the plasmids used to generate telomerase extracts.

Author Contributions

Conceptualization: Derek J. Taylor.

Data curation: Wilnelly Hernandez-Sanchez, Brian Plucinsky, Nelson Garcia-Vazquez, Nathaniel J. Robinson, Emmanuel Skordalakes.

Formal analysis: Wilnelly Hernandez-Sanchez, Brian Plucinsky, Emmanuel Skordalakes, Derek J. Taylor.

Funding acquisition: Emmanuel Skordalakes, Derek J. Taylor.

Investigation: Wilnelly Hernandez-Sanchez, Wei Huang, Brian Plucinsky, Nathaniel J. Robinson, William P. Schiemann, Emmanuel Skordalakes, Derek J. Taylor.

Resources: Anthony J. Berdis.

Supervision: Emmanuel Skordalakes, Derek J. Taylor.

Validation: Wilnelly Hernandez-Sanchez, Brian Plucinsky, Anthony J. Berdis, Emmanuel Skordalakes.

Visualization: Wei Huang, Brian Plucinsky, Nelson Garcia-Vazquez, Emmanuel Skordalakes.

Writing – original draft: Wilnelly Hernandez-Sanchez, Wei Huang, Derek J. Taylor.

Writing – review & editing: Wilnelly Hernandez-Sanchez, Brian Plucinsky, Anthony J. Berdis, Emmanuel Skordalakes, Derek J. Taylor.

References

1. Nandakumar J, Cech TR. Finding the end: recruitment of telomerase to telomeres. Nat Rev Mol Cell Biol. 2013; 14(2):69–82. https://doi.org/10.1038/nrm3505 PMID: 23299958
2. de Lange T. Shelterin: the protein complex that shapes and safeguards human telomeres. Genes Dev. 2005; 19(18):2100–10. https://doi.org/10.1101/gad.1346005 PMID: 16166375
3. Levy MZ, Allsopp RC, Futcher AB, Greider CW, Harley CB. Telomere end-replication problem and cell aging. J Mol Biol. 1992; 225(4):951–60. PMID: 1613801
4. Hayflick L. The Limited in Vitro Lifetime of Human Diploid Cell Strains. Exp Cell Res. 1965; 37:614–36. PMID: 14315085
5. Blackburn EH. Telomere states and cell fates. Nature. 2000; 408(6808):53–6. https://doi.org/10.1038/35040500 PMID: 11081503
6. Shay JW, Bacchetti S. A survey of telomerase activity in human cancer. Eur J Cancer. 1997; 33 (5):787–91. https://doi.org/10.1016/S0959-8049(97)00062-2 PMID: 9282118
7. Lingner J, Hughes TR, Shevchenko A, Mann M, Lundblad V, Cech TR. Reverse transcriptase motifs in the catalytic subunit of telomerase. Science. 1997; 276(5312):561–7. PMID: 9110970
8. Greider CW, Blackburn EH. A telomeric sequence in the RNA of Tetrahymena telomerase required for telomere repeat synthesis. Nature. 1989; 337(6205):331–7. https://doi.org/10.1038/337331a0 PMID: 2463488
9. Greider CW, Blackburn EH. Identification of a specific telomere terminal transferase activity in Tetrahymena extracts. Cell. 1985; 43(2 Pt 1):405–13. PMID: 3907856
10. Zhang X, Mar V, Zhou W, Harrington L, Robinson MO. Telomere shortening and apoptosis in telomerase-inhibited human tumor cells. Genes Dev. 1999; 13(18):2388–99. PMID: 10500096
11. Gryaznov SM, Jackson S, Dikmen G, Harley C, Herbert BS, Wright WE, et al. Oligonucleotide conjugate GRN163L targeting human telomerase as potential anticancer and antimetastatic agent. Nucleosides Nucleotides Nucleic Acids. 2007; 26(10–12):1577–9. https://doi.org/10.1080/15257770701547271 PMID: 18066830
12. Thompson PA, Drissi R, Muscal JA, Panditharatna E, Fouladi M, Ingle AM, et al. A phase I trial of imetelstat in children with refractory or recurrent solid tumors: a Children's Oncology Group Phase I Consortium Study (ADVL1112). Clin Cancer Res. 2013; 19(23):6578–84. https://doi.org/10.1158/1078-0432.CCR-13-1117 PMID: 24097866
13. Rossi A, Russo G, Puca A, La Montagna R, Caputo M, Mattioli E, et al. The antiretroviral nucleoside analogue Abacavir reduces cell growth and promotes differentiation of human medulloblastoma cells. International Journal of Cancer. 2009; 125(1):235–43. https://doi.org/10.1002/ijc.24331 PMID: 19358275

14. Jordheim LP, Durantel D, Zoulim F, Dumontet C. Advances in the development of nucleoside and nucleotide analogues for cancer and viral diseases. Nature reviews Drug discovery. 2013; 12(6):447–64. https://doi.org/10.1038/nrd4010 PMID: 23722347

15. Dasari A, Choi JS, Berdis AJ. Chemotherapeutic Intervention by Inhibiting DNA Polymerases. DNA Repair in Cancer Therapy: Molecular Targets and Clinical Applications, 2nd Edition. 2016:179–224.

16. Yarchoan R, Klecker RW, Weinhold KJ, Markham PD, Lyerly HK, Durack DT, et al. Administration of 3'-azido-3'-deoxythymidine, an inhibitor of HTLV-III/LAV replication, to patients with AIDS or AIDS-related complex. Lancet. 1986; 1(8481):575–80. PMID: 2869302

17. Fischl MA, Richman DD, Grieco MH, Gottlieb MS, Volberding PA, Laskin OL, et al. The efficacy of azidothymidine (AZT) in the treatment of patients with AIDS and AIDS-related complex. A double-blind, placebo-controlled trial. N Engl J Med. 1987; 317(4):185–91. https://doi.org/10.1056/NEJM198707233170401 PMID: 3299089

18. Mitchell M, Gillis A, Futahashi M, Fujiwara H, Skordalakes E. Structural basis for telomerase catalytic subunit TERT binding to RNA template and telomeric DNA. Nature Structural & Molecular Biology. 2010; 17(4):513–U163.

19. Strahl C, Blackburn EH. The effects of nucleoside analogs on telomerase and telomeres in Tetrahymena. Nucleic Acids Res. 1994; 22(6):893–900. PMID: 8152919

20. Strahl C, Blackburn EH. Effects of reverse transcriptase inhibitors on telomere length and telomerase activity in two immortalized human cell lines. Mol Cell Biol. 1996; 16(1):53–65. PMID: 8524329

21. Liu X, Takahashi H, Harada Y, Ogawara T, Ogimura Y, Mizushina Y, et al. 3'-Azido-2',3'-dideoxynucleoside 5'-triphosphates inhibit telomerase activity in vitro, and the corresponding nucleosides cause telomere shortening in human HL60 cells. Nucleic Acids Res. 2007; 35(21):7140–9. https://doi.org/10.1093/nar/gkm859 PMID: 17942424

22. Clarke E, Rice GC, Weeks RS, Jenkins N, Nelson R, Bianco JA, et al. Lisofylline inhibits transforming growth factor beta release and enhances trilineage hematopoietic recovery after 5-fluorouracil treatment in mice. Cancer Res. 1996; 56(1):105–12. PMID: 8548748

23. Miller KD, Loehrer PJ, Gonin R, Weber G, Ansari R, Pletcher W, et al. A phase II study of weekly oral methotrexate and zidovudine (AZT) in advanced adenocarcinoma of the pancreas and hepatocellular carcinoma. Invest New Drugs. 1996; 14(2):207–12. PMID: 8913842

24. Marchbanks K, Dudley MN, Posner MR, Darnowski J. Pharmacokinetics and pharmacodynamics of high-dose zidovudine administered as a continuous infusion in patients with cancer. Pharmacotherapy. 1995; 15(4):451–7. PMID: 7479197

25. Posner MR, Darnowski JW, Weitberg AB, Dudley MN, Corvese D, Cummings FJ, et al. High-dose intravenous zidovudine with 5-fluorouracil and leucovorin. A phase I trial. Cancer. 1992; 70(12):2929–34. PMID: 1451076

26. Johnson AA, Johnson KA. Fidelity of nucleotide incorporation by human mitochondrial DNA polymerase. J Biol Chem. 2001; 276(41):38090–6. https://doi.org/10.1074/jbc.M106045200 PMID: 11477093

27. Lim SE, Copeland WC. Differential incorporation and removal of antiviral deoxynucleotides by human DNA polymerase gamma. J Biol Chem. 2001; 276(26):23616–23. https://doi.org/10.1074/jbc.M101114200 PMID: 11319228

28. Greider CW. Telomerase is processive. Mol Cell Biol. 1991; 11(9):4572–80. PMID: 1875940

29. Nakamura TM, Morin GB, Chapman KB, Weinrich SL, Andrews WH, Lingner J, et al. Telomerase catalytic subunit homologs from fission yeast and human. Science. 1997; 277(5328):955–9. PMID: 9252327

30. Kelleher C, Teixeira MT, Forstemann K, Lingner J. Telomerase: biochemical considerations for enzyme and substrate. Trends Biochem Sci. 2002; 27(11):572–9. PMID: 12417133

31. Nakamura TM, Cech TR. Reversing time: origin of telomerase. Cell. 1998; 92(5):587–90. PMID: 9506510

32. Motea EA, Lee I, Berdis AJ. Insights into the roles of desolvation and pi-electron interactions during DNA polymerization. Chembiochem: a European journal of chemical biology. 2013; 14(4):489–98. https://doi.org/10.1002/cbic.201200649 PMID: 23404822

33. Golden J, Motea E, Zhang X, Choi JS, Feng Y, Xu Y, et al. Development and characterization of a non-natural nucleoside that displays anticancer activity against solid tumors. ACS chemical biology. 2013; 8 (11):2452–65. https://doi.org/10.1021/cb400350h PMID: 23992753

34. Zhang X, Lee I, Berdis AJ. The use of nonnatural nucleotides to probe the contributions of shape complementarity and pi-electron surface area during DNA polymerization. Biochemistry. 2005; 44 (39):13101–10. https://doi.org/10.1021/bi050585f PMID: 16185078

35. Vineyard D, Zhang X, Donnelly A, Lee I, Berdis AJ. Optimization of non-natural nucleotides for selective incorporation opposite damaged DNA. Organic & biomolecular chemistry. 2007; 5(22):3623–30.

36. Motea EA, Lee I, Berdis AJ. Quantifying the energetic contributions of desolvation and pi-electron density during translesion DNA synthesis. Nucleic Acids Res. 2011; 39(4):1623–37. https://doi.org/10.1093/nar/gkq925 PMID: 20952399

37. Cristofari G, Lingner J. Telomere length homeostasis requires that telomerase levels are limiting. Embo J. 2006; 25(3):565–74. https://doi.org/10.1038/sj.emboj.7600952 PMID: 16424902

38. Freudenthal BD, Beard WA, Wilson SH. New structural snapshots provide molecular insights into the mechanism of high fidelity DNA synthesis. DNA repair. 2015; 32:3–9. https://doi.org/10.1016/j.dnarep.2015.04.007 PMID: 26002198

39. Perera L, Freudenthal BD, Beard WA, Pedersen LG, Wilson SH. Revealing the role of the product metal in DNA polymerase beta catalysis. Nucleic Acids Res. 2017; 45(5):2736–45. https://doi.org/10.1093/nar/gkw1363 PMID: 28108654

40. Patra A, Zhang Q, Lei L, Su Y, Egli M, Guengerich FP. Structural and kinetic analysis of nucleoside triphosphate incorporation opposite an abasic site by human translesion DNA polymerase eta. J Biol Chem. 2015; 290(13):8028–38. https://doi.org/10.1074/jbc.M115.637561 PMID: 25666608

41. Jansson LI, Akiyama BM, Ooms A, Lu C, Rubin SM, Stone MD. Structural basis of template-boundary definition in Tetrahymena telomerase. Nat Struct Mol Biol. 2015; 22(11):883–8. https://doi.org/10.1038/nsmb.3101 PMID: 26436828

42. Nguyen THD, Tam J, Wu RA, Greber BJ, Toso D, Nogales E, et al. Cryo-EM structure of substrate-bound human telomerase holoenzyme. Nature. 2018; 557(7704):190–5.

43. Jiang J, Wang Y, Susac L, Chan H, Basu R, Zhou ZH, et al. Structure of Telomerase with Telomeric DNA. Cell. 2018; 173(5):1179–90 e13.

44. Scruggs ER, Dirks Naylor AJ. Mechanisms of zidovudine-induced mitochondrial toxicity and myopathy. Pharmacology. 2008; 82(2):83–8. https://doi.org/10.1159/000134943 PMID: 18504416

45. Gomez DE, Armando RG, Alonso DF. AZT as a telomerase inhibitor. Front Oncol. 2012; 2:113. https://doi.org/10.3389/fonc.2012.00113 PMID: 22973556

46. Nickel W, Austermann S, Bialek G, Grosse F. Interactions of azidothymidine triphosphate with the cellular DNA polymerases alpha, delta, and epsilon and with DNA primase. J Biol Chem. 1992; 267(2):848–54. PMID: 1730673

47. Copeland WC, Chen MS, Wang TS. Human DNA polymerases alpha and beta are able to incorporate anti-HIV deoxynucleotides into DNA. J Biol Chem. 1992; 267(30):21459–64. PMID: 1400458

48. Lynx MD, Bentley AT, McKee EE. 3'-Azido-3'-deoxythymidine (AZT) inhibits thymidine phosphorylation in isolated rat liver mitochondria: a possible mechanism of AZT hepatotoxicity. Biochem Pharmacol. 2006; 71(9):1342–8. https://doi.org/10.1016/j.bcp.2006.01.003 PMID: 16472780

49. Lai CK, Mitchell JR, Collins K. RNA binding domain of telomerase reverse transcriptase. Mol Cell Biol. 2001; 21(4):990–1000. https://doi.org/10.1128/MCB.21.4.990-1000.2001 PMID: 11158287

50. Gillis AJ, Schuller AP, Skordalakes E. Structure of the Tribolium castaneum telomerase catalytic subunit TERT. Nature. 2008; 455(7213):633–U36. https://doi.org/10.1038/nature07283 PMID: 18758444

51. Rouda S, Skordalakes E. Structure of the RNA-binding domain of telomerase: implications for RNA recognition and binding. Structure. 2007; 15(11):1403–12. https://doi.org/10.1016/j.str.2007.09.007 PMID: 17997966

52. Das R, Laederach A, Pearlman SM, Herschlag D, Altman RB. SAFA: semi-automated footprinting analysis software for high-throughput quantification of nucleic acid footprinting experiments. RNA. 2005; 11(3):344–54. https://doi.org/10.1261/rna.7214405 PMID: 15701734

53. Johnson KA. Fitting enzyme kinetic data with KinTek Global Kinetic Explorer. Methods in enzymology. 2009; 467:601–26. https://doi.org/10.1016/S0076-6879(09)67023-3 PMID: 19897109

54. Kabsch W. Xds. Acta Crystallogr D Biol Crystallogr. 2010; 66(Pt 2):125–32. https://doi.org/10.1107/S0907444909047337 PMID: 20124692

55. Potterton E, Briggs P, Turkenburg M, Dodson E. A graphical user interface to the CCP4 program suite. Acta Crystallogr D Biol Crystallogr. 2003; 59(Pt 7):1131–7.

56. Adams PD, Afonine PV, Bunkoczi G, Chen VB, Davis IW, Echols N, et al. PHENIX: a comprehensive Python-based system for macromolecular structure solution. Acta Crystallogr D Biol Crystallogr. 2010; 66(Pt 2):213–21.

57. Emsley P, Cowtan K. Coot: model-building tools for molecular graphics. Acta Crystallogr D Biol Crystallogr. 2004; 60(Pt 12 Pt 1):2126–32. https://doi.org/10.1107/S0907444904019158 PMID: 15572765

58. Murshudov GN, Vagin AA, Dodson EJ. Refinement of macromolecular structures by the maximum-likelihood method. Acta Crystallogr D Biol Crystallogr. 1997; 53(Pt 3):240–55.